

Optimized Triple-Slot Patch Antenna with Electromagnetic Band Gap Structures for Enhanced Performance

Original Scientific Paper

Gowri Chaduvula*

Department of Electronics and Communication Engineering,
Jawaharlal Nehru Technological University, Kakinada,
Andhra Pradesh, India
gowrich.ece@gmail.com

Leela Kumari B

JNTU Kakinada,
Faculty of Engineering, Department of Electronics and Communication
Kakinada, Andhra Pradesh, India
leela8821@yahoo.com

*Corresponding author

Abstract – This paper presents an antenna integrated with an Electromagnetic Bandgap (EBG) structure to enhance its radiation performance compared to a conventional antenna. MEBG (Mushroom EBG) and EEBG (Edge via EBG) structures are analyzed, integrating MEBG with the triple-slot patch antenna, which demonstrates superior performance. Using the same conventional dimensions, the proposed antenna achieves a gain of 6.15 dB, a directivity of 7.51 dB, and a return loss of 37 dB at 5.2 GHz, providing a 1.92 dB gain improvement over the conventional design. This design is simulated using the HFSS software. The measurement results are validated with simulation results. The fabricated, compact antenna can be used for IoT applications at 5.2 GHz.

Keywords: patch antenna, EBG, triple-slot, MEBG, EEBG, gain, IoT

Received: January 1, 2025; Received in revised form: April 5, 2025; Accepted: April 9, 2025

1. INTRODUCTION

Today, with the evolution of wireless communication technologies, billions of IoT devices are connected to the internet, exchanging information wirelessly [1]. The key requirement for these systems is the integration of compact, high-performance antennas to ensure reliable data transfer [2]. Antennas are the primary components used to transmit or receive information in wireless communication, making their design a vital factor in optimizing IoT connectivity. Microstrip patch antennas are preferred in wireless applications since they are lightweight, small, easy to fabricate, and adaptable to feeding networks [3].

There is a high demand for IoT applications, hence, research is being put forth for compact, high-gain antenna designs that can serve longer distances with improved bandwidth. However, conventional microstrip patch antennas suffer from low gain and low bandwidth. In the literature, several strategies have been applied to antennas to improve their radiation charac-

teristics, making them appropriate for IoT applications. In [4], an L-slotted patch antenna is designed for IoT applications at 2.4 GHz. Improved patch antenna performance is achieved by incorporating slots in the patch to enable operation at 868 MHz for IoT applications [5]. A pixel antenna array is designed for high-gain IoT applications [6]. The U-slot microstrip antenna is designed for IoT applications [7]. DGS, combined with slots in patch antenna, is used for IoT applications [8]. However, designing compact antennas for effective integration with IoT devices is challenging.

Designing antennas on high permittivity substrates results in compact sizes, but it introduces challenges related to the generation of surface waves [9]. Patch antenna performance can be significantly affected by surface waves travelling along the interface between metal and dielectric boundaries. This dispersion causes distortion in radiation patterns and leads to multipath interference, resulting in issues like deep nulls, increased back lobe radiation, reduced gain, and overall decreased performance [10].

A powerful and widely adopted technique for mitigating surface waves is the use of Electromagnetic Band Gap (EBG) structures. EBG structures are defined as “artificial periodic objects that prevent the propagation of electromagnetic waves in a specified range of frequencies for all incident angles and polarization states” [11]. Due to their unique bandgap features, these are considered a special type of metamaterial. Additionally, EBGs exhibit high-impedance surface properties and artificial magnetic conductor (AMC) behavior, making them valuable in antenna engineering and microwave circuits. EBGs are classified based on their geometry into 1D, 2D, and 3D types. Mushroom EBGs (MEBGs) are the most popular choice in two-dimensional structures for effectively reducing surface waves. As discussed in the literature, novel EBG structures are integrated with antenna configurations to enhance performance. Improved isolation and lower radar cross-sections are achieved with frequency-selective surfaces in MIMO antennas [12]. TVDS-EBG is implemented for bandwidth enhancement of the UWB monopole antenna [13]. Isolation improvement in dual-band meander lines has been achieved using split EBG in multiple antenna systems [14].

In particular, several EBG structures are employed to increase the gain of the patch antenna. Mushroom-like EBG structures are integrated with patch antennas to enhance performance at 28 GHz [15]. Improved patch antenna performance for C-band applications is achieved by incorporating mushroom EBGs, which successfully suppress surface waves at 6 GHz [16]. A polarization-dependent metamaterial surface made of EBG structures provides high-gain, low-RCS patch antenna at 3.25 GHz [17]. Reducing the propagation modes of surface waves, thereby enhancing the gain of a patch antenna is achieved by integrating an I-shaped EBG structures with antenna [18]. Gain enhancement for a patch antenna fed by a coaxial probe is achieved through the utilization of L-slotted EBG structures at 5.8 GHz [19]. Performance improvement in terms of gain and radiation pattern of patch antennas is accomplished by using steps like EBG at 5.8 GHz [20]. Fractal-shaped EBG is utilized for gain enhancement of patch antennas and improves the directionality by successfully suppressing the surface waves [21].

From the above-mentioned literature, it is noted that improving the antenna performance requires a larger number of EBG cells, leading to increased design complexity. However, for specific IoT applications, antenna design requires high directivity without increasing the size operated to a particular band. The proposed antenna incorporates a triple-slot design integrated with MEBGs, resulting in a substantial gain improvement. While this design is simple, the triple-slot configuration is combined with a minimal number of MEBGs with improved performance. The results, validated through both simulation and fabrication, demonstrate that this approach provides an optimized balance between performance enhancement and design simplicity, making it suited for IoT-enabled wireless applications.

2. ANTENNA DESIGN WITH EBG STRUCTURES

This section improves the gain by incorporating EBG cells around the patch antenna at the resonant frequency of 5.2 GHz.

2.1. REFERENCE ANTENNA DESIGN

A basic microstrip antenna with a rectangular patch is designed to operate at 5.2 GHz. The radiating patch is mounted on an FR-4 substrate with a height of 1.6 mm. A microstrip feed line is contacted directly to the patch. Basic antenna dimensions are calculated using equations and tabulated in Table 1, and the layout is displayed in Fig. 1. This antenna serves as a reference to compare the performance with the proposed configurations in the subsequent section [22].

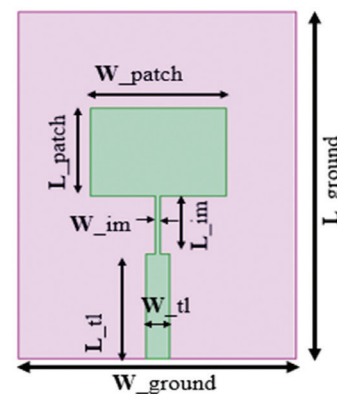


Fig. 1. Design of conventional microstrip patch antenna

Table 1. Specifications of conventional antenna

Parameters	Dimensions (mm*mm)
Substrate	35.9 * 58.9
Ground	35.9 * 58.9
Patch	12.56 * 17.56
$L_{im} * W_{im}$	7.29 * 0.723
$L_{tl} * W_{tl}$	14.59 * 3.059

Another modified antenna incorporates slots in a conventional patch antenna to improve performance. This modified antenna has three rectangular slots that are each 6 by 2 mm² in size. A triple-slot patch antenna layout is depicted in Fig. 2.

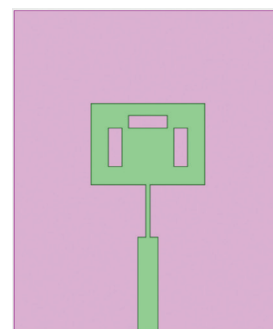


Fig. 2. Triple-slot patch antenna design

2.2. DESIGN AND ANALYSIS OF EBG UNIT CELL

This study includes designing and analyzing both Mushroom EBG (MEBG) and Edge via EBG (EEBG) structures. Initially, EBG unit cell characteristics are thoroughly explained, and later, the design and analysis of both EBG cells are explored in this section.

Basic EBG structures are typically arranged periodically and include four main parts: a metallic patch, a ground plane, a substrate, and a vertical connecting rod extending through the substrate. These periodic EBG structures act as high-impedance surfaces, effectively preventing surface waves from entering inside a specific bandgap. Analysis of a larger array is quite challenging; a simple way to find the characteristics is by applying the periodic boundary condition (PBC) to a unit cell. When the periodicity of the EBG structures is shorter than λ (wavelength), they are referred to as lumped elements (LC) [23]. It functions as a parallel resonance LC filter. An LC filter can exhibit the characteristics of the EBG structure. The presence of vias is crucial in the formation of the well-known two-dimensional mushroom EBG (MEBG). In MEBG, a central via connects the patch to the ground plane. This enables the current to flow, producing inductance (L) and capacitance (C) between the metal planes and the dielectric. The periodic arrangement of MEBG, along with the equivalent circuit diagram, is illustrated in Fig. 3.

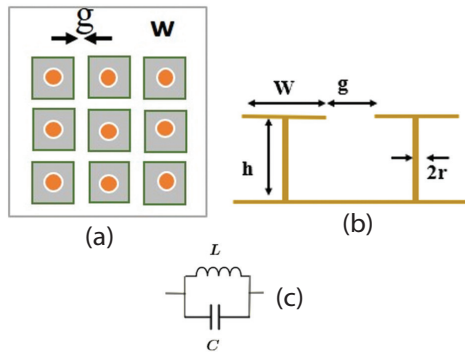


Fig. 3. MEBG unit cells (a) top view (b) side view (c) equivalent circuit

The L and C values determine the frequency band gap, resonant frequency, and surface impedance. These parameters are calculated using the following formulae [24].

$$L = \mu_0 h \quad (1)$$

$$C = \frac{w\epsilon_0(1+\epsilon_r)}{h} \cosh^{-1} \left(\frac{2w+g}{g} \right) \quad (2)$$

$$f_0 = 1 / 2\pi(\sqrt{LC}) \quad (3)$$

$$Z = \frac{j\omega L}{1-\omega^2 LC} \quad (4)$$

Based on the parameters of EBG, which include patch width (w), gap between cells (g), and substrate thickness (h), operating frequency and forbidden band-

gap are determined. Equation (4) shows that at the resonant frequency, the EBG creates a high-impedance state, which blocks surface waves [25].

In the case of EEBG, the via is moving from the center to the border of the patch. The arrangement of EEBG is shown in Fig. 4. Via routes from the center to the edge, it extends the electrical path to carry out the high impedance transformation [26].

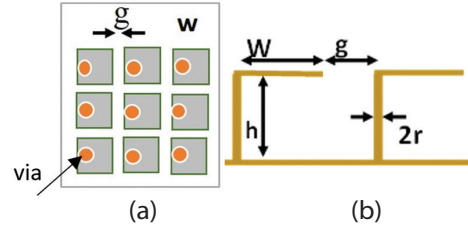


Fig. 4. EEBG unit cells (a) front view (b) side view

Both the MEBG and the EEBG are designed to achieve an operating frequency of 5.2 GHz, utilizing HFSS software for implementation. In both scenarios, the unit cell of the metallic patch features a square configuration. The metallic patch for both MEBG and EEBG is mounted on an FR-4 substrate with a height of 1.6 mm. This simulation is conducted using periodic boundary conditions (PBCs), which effectively replicate an infinitely periodic structure on all four sides of the cell, as shown in Fig. 5 for MEBG and EEBG. To establish the periodic boundary conditions in HFSS, apply master-slave settings to all four sides of the unit cell. A perfectly matched layer (PML) composed of anisotropic material serves as a boundary at the top of the model volume to prevent reflections and ensure the effective absorption of outgoing electromagnetic waves. The observation plane is positioned at a height nearly ten times greater than the substrate height to reduce the effects of higher-order modes in the results of the EBG unit cell [27]. Using a floquet port in HFSS, plane waves are incident from the top of the EBG cell.

The optimized MEBG and EEBG designs operate at 5.2 GHz. MEBG has a patch width of 8.7 mm, a via radius of 0.2 mm, and a 0.3 mm gap, while EEBG features a 5.4 mm patch width, a 0.3 mm via radius, and a 0.6 mm gap.

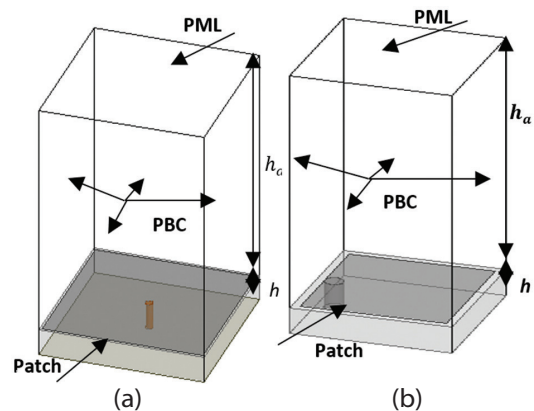


Fig. 5. Simulation setup (a) MEBG unit cell (b) EEBG unit cell

The forbidden band characteristics and operating frequency for these structures are determined by either the reflection phase or the dispersion diagram. A dispersion diagram interprets the relation between wave frequencies and wave numbers. In the case of the reflection phase, the phase of surface impedance varies concerning frequency from 180° to -180° . AMC features appear in the range of 90° to -90° , where surface currents shift phase to support antenna currents, creating a stopband. Fig. 6 illustrates the reflection phase of both MEBG and EEBG.

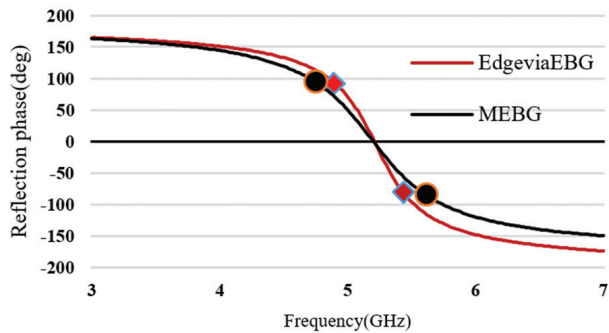


Fig. 6. Reflection phase vs frequency for MEBG and EEBG

From Fig. 6, both the EBGs having a 0° reflection are at 5.2 GHz. The band gap of MEBG is exhibited at 4.78-5.65 GHz. Whereas EEBG exhibits a bandgap around 4.91-5.47 GHz. Compared to MEBG, EEBG exhibits a narrow bandwidth; it shows nearly a 6% decrement in the band gap.

2.3. INTEGRATION OF EBG WITH ANTENNA

In this section, different proposed configurations of antennas are integrated with EBG unit cells while maintaining the same dimensions. For all the configurations the substrate dimensions are $40.8 \times 50.5 \times 1.6 \text{ mm}^3$. These configurations include a conventional antenna with EEBG, a conventional antenna with MEBG, a triple-slot antenna with EEBG, and a triple-slot antenna with MEBG, as shown in Fig. 7.

The first configuration is designed by incorporating EEBG cells around a conventional antenna. The patch dimensions are not changed, and feeding is also the same as that given by the edge feed technique. The gap between EBG cells is kept at 3 mm, and 19 EEBG cells are positioned on the same substrate, as shown in Fig. 7(a).

The second configuration consists of the conventional patch, surrounded by MEBG unit cells, which forms a new design known as the conventional patch antenna with MEBG. The gap between EBG cells is kept at 1 mm, and 12 MEBG cells are positioned on the same substrate. The layout of this new antenna is shown in Fig. 7(b).

The third proposed configuration consists of the conventional patch antenna with EEBG substituted by incorporating a triple slot in the patch. As seen in

Fig. 7(c), this transformation produces a unique antenna known as the triple-slot patch antenna with EEBG. Another configuration is that the conventional antenna is replaced by a triple-slot patch antenna and surrounded with MEBG unit cells. This became a new antenna triple-slot patch antenna with MEBG, as shown in Fig. 7(d).

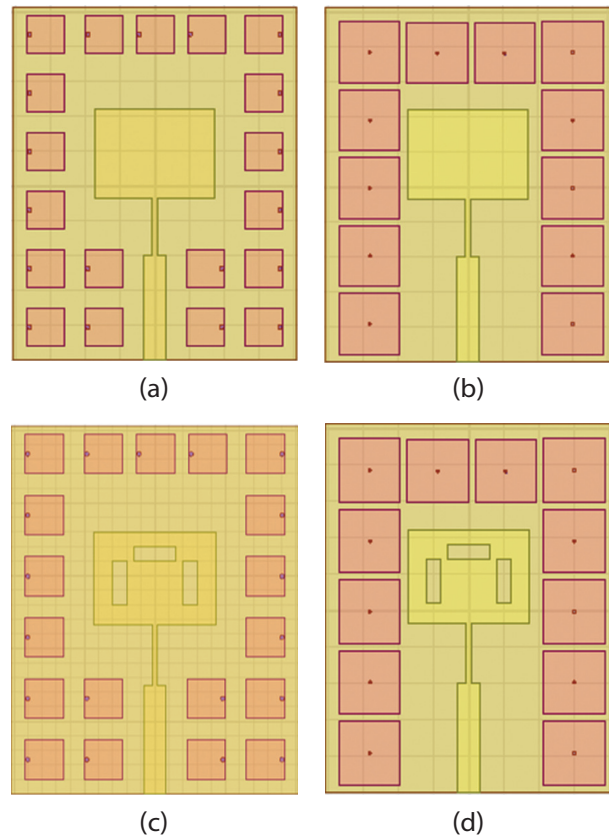


Fig. 7. Design of proposed configurations
(a) Layout of conventional patch antenna with EEBG
(b) Layout of conventional patch antenna with MEBG
(c) Layout of triple slot patch antenna with EEBG
(d) Layout of triple slot patch antenna with MEBG

3. RESULTS AND DISCUSSION

This section discusses the simulation results of all design configurations, including the best-performing prototype, which is validated through fabrication results.

3.1. SIMULATION RESULTS

The design of six different configurations of antennas is done using HFSS software. The simulated findings are analyzed in this section. The configurations include a conventional antenna, a triple slot antenna, a conventional antenna with EEBG, a conventional antenna with MEBG, a triple-slot antenna with EEBG, and a triple-slot antenna with MEBG. The simulation findings for each configuration address basic antenna performance parameters, including gain, peak directivity, reflection coefficient (S_{11}) or return loss, and voltage standing wave ratio (VSWR). The quantitative parameters of the different antenna configurations are tabulated in Table 2.

Simulated return loss curve changes with the frequency for each of the six designs are illustrated in Fig. 8, where the conventional antenna and its EEBG and MEBG are radiated at a 5.2 GHz resonant frequency. Whereas a triple-slot antenna and its EEBG and MEBG slightly move the operating frequency to 5 GHz because slots create an additional current path, which increases the electrical length of a patch; hence, the resonant frequency decreases. The simulated S11 parameter for each configuration is as follows: -17.8 dB (conventional), -25.7 dB (triple slot), -29.3 dB (conventional with EEBG), -20.8 dB (conventional with MEBG), -31.3 dB (triple-slot with EEBG), and -37.2 dB (triple-slot with MEBG).

An excellent impedance match between the patch and feedline is achieved when the triple-slot antenna with MEBG exhibits a steep decrease in the reflection coefficient when compared to the other configurations. There is an 87% incremental return loss when comparing a conventional antenna to a triple-slot antenna with MEBG. According to the VSWR values obtained from Fig. 9, MEBG performs better than EEBG in attaining impedance matching, which is a crucial component of antenna design.

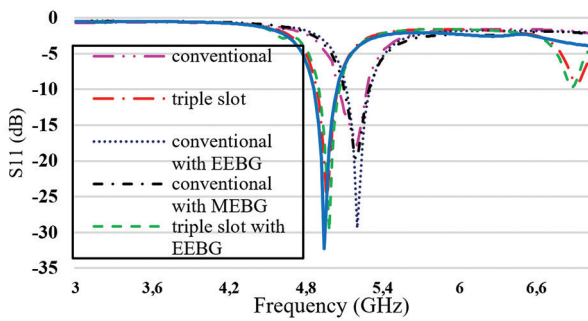


Fig. 8. Return loss vs frequency for all antenna configurations

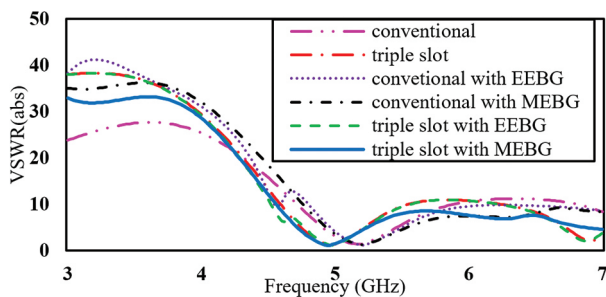


Fig. 9. VSWR vs frequency for all antenna configurations

The radiation pattern, which describes the transmission/reception power from an antenna that varies in different directions, gives important information on how the antenna is directing the power, polarization, and gain properties. The E plane ($\varphi=0^\circ$) and H plane ($\varphi=90^\circ$) of the radiation pattern are simulated for conventional and triple-slot antennae as shown in Fig. 10(a), conventional with EEBG and MEBG, as shown in Fig. 10(b).

E & H plane of triple-slot antenna and it's with EEBG and MEBG, as depicted in Fig. 10(c) and 10(d).

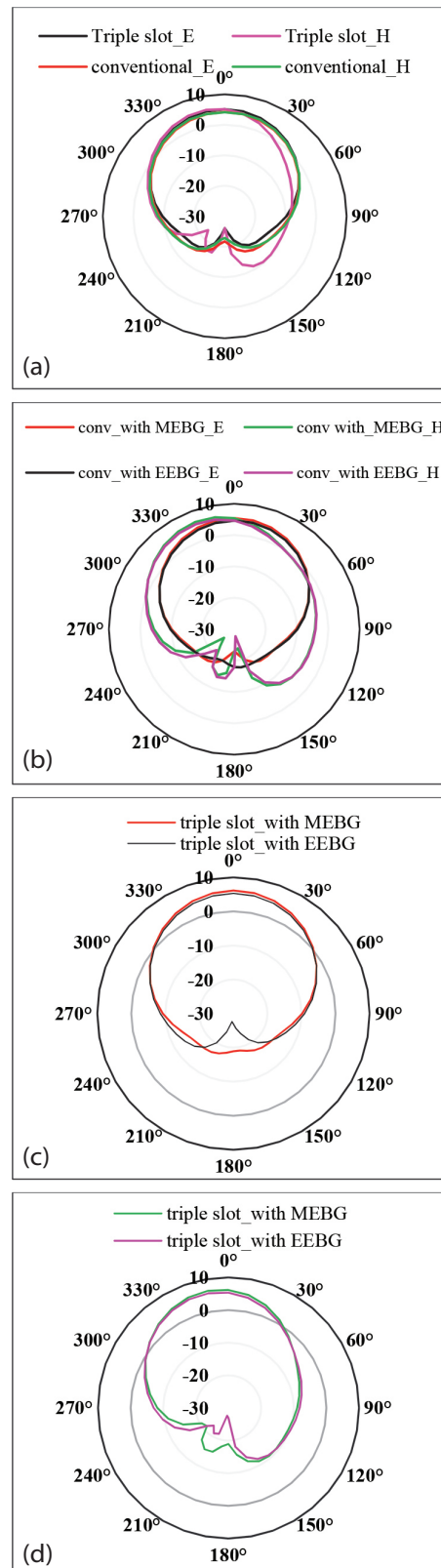


Fig. 10. Radiation plots (a) E, H plane for conventional and triple-slot antenna (b) E, H radiation planes for a conventional antenna with EEBG & MEBG (c) E plane for triple-slot antenna with EEBG & MEBG (d) H plane for triple-slot antenna with EEBG & MEBG

Both the planes of the conventional and triple-slot antennas are similar. The addition of slots in the conventional antenna leads to improved gain and reduced back lobe radiation. When comparing EEBG with MEBG, MEBG further reduces back lobe radiation and enhances gain. Fig. 10 illustrates the achievement of a unidirectional pattern for the triple-slot antenna with MEBG, showcasing improved radiation performance compared to EEBG. There is a substantial improvement in gain quantity for a triple-slot antenna with an MEBG compared with a conventional antenna as depicted in Fig. 11(a). When the MEBG cells are included in a triple slot antenna, broadside gain is raised from 4.22 dB to 6.15 dB. The proposed antenna's gain varies with frequency, as illustrated in Fig. 11(b). The three-dimensional radiation pattern at 5.2 GHz is shown in Fig. 12, demonstrating that the realized gain reaches 6.43 dBi.

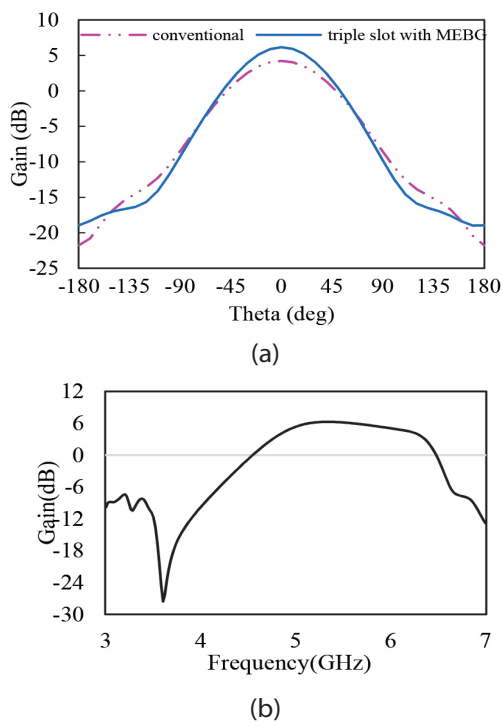


Fig. 11. Gain plot (a) gain varies with spatial coordinates for conventional and proposed antenna (b) gain varies with frequency for the proposed antenna

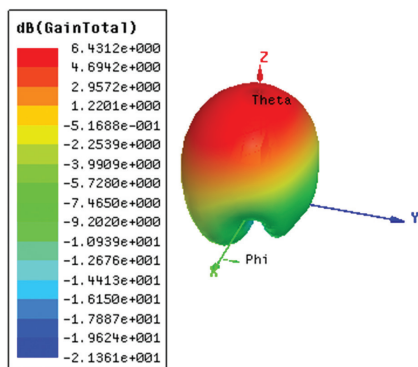


Fig. 12. The 3-D gain plot of the proposed triple-slot antenna with MEBG

Table 2. Antenna parameters of all configurations

Antenna configurations	S11 (dB)	VSWR (abs)	Gain (dB)	Frequency (GHz)	Peak Directivity (dB)
Conventional	-17.8	1.29	4.22	5.2	5.3
Triple-slot	-25.7	1.12	5.11	4.96	6.64
Conventional with EEBG	-29.3	1.07	4.63	5.2	6.26
Conventional with MEBG	-20.8	1.21	5.38	5.2	6.73
Triple-slot with EEBG	-31.3	1.07	5.31	4.97	6.96
Triple-slot with MEBG	-37.2	1.03	6.15	4.94	7.51

3.2. FABRICATION RESULTS

The best given simulated antenna is a triple-slot antenna with MEBG fabricated with the specifications ($\epsilon_r = 4.4$, $h = 1.6$ mm, $\tan \delta = 0.02$). It features a 50-ohm SMA connector attached at the end of the feed line. Measurements are conducted using an Agilent N5247A network analyzer, which supports a maximum frequency of up to 18 GHz. Fig.13 illustrates the front and back views of the fabricated antenna along with the measurement setup for return loss analysis. The main challenge in fabricating MEBG structures is achieving precise etching, especially in maintaining gap width and via placements, which were accomplished using UV photoresist etching. Dipping of copper wires into the vias increased complexity, resulting in fabrication tolerances and measurement errors. Impedance mismatches from SMA connectors were addressed through calibrated soldering and VNA testing. These steps ensured that the fabricated prototype closely matched simulations, validating the design. The measured and simulated return loss curves for the triple-slot patch antenna with MEBG are presented in Fig.14.

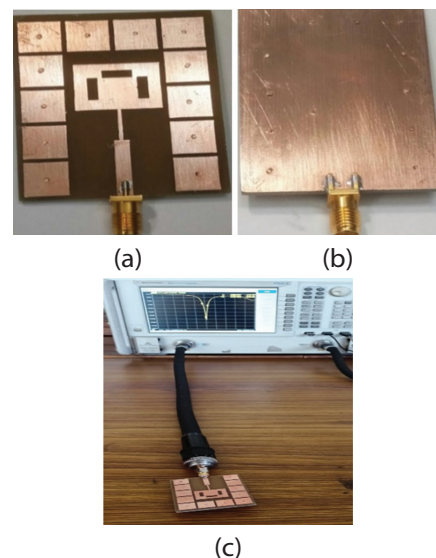


Fig.13. Proposed constructed antenna (a) top view (b) rear view (c) measurement setup of fabricated antenna with VNA

It appears that the operational frequency of the manufactured antenna is merely shifted to 5 GHz from 5.2 GHz. The fabricated antenna produces a return loss of 44.82 dB at an operating frequency of 5 GHz. From conventional to fabricated antenna, the return loss is increased from 17.8 dB to 44.2 dB.

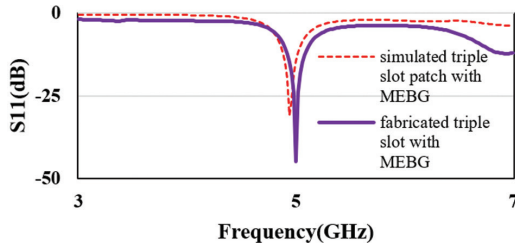


Fig.14. Plot of simulated vs fabricated results of S11 w.r.t frequency

Fig. 15 displays the E-plane and H-plane radiation patterns for the fabricated antenna measured in the anechoic chamber. Both the simulated and developed antennas produce and match the far-field radiation pattern of the E and H planes acceptably, and the gain of the proposed antenna is 6.15 dB. A minor lobe is slightly increased compared with simulation results due to measurement errors. Introducing a conventional slot surrounded by MEBG raises the gain quantity by 1.93 dB compared to the conventional antenna, as mentioned in the measured gain plot at 5.2 GHz, and efficiency is about 70%, as shown in Fig. 19(c). The suggested antenna is compact and has better performance. Table 3 compares the gain augmentation attained by the suggested antenna with other antennas available in the existing research, accounting for the quantity of EBG cells used.

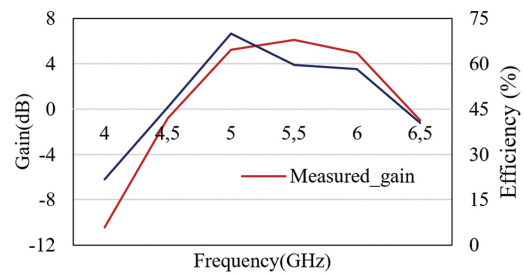
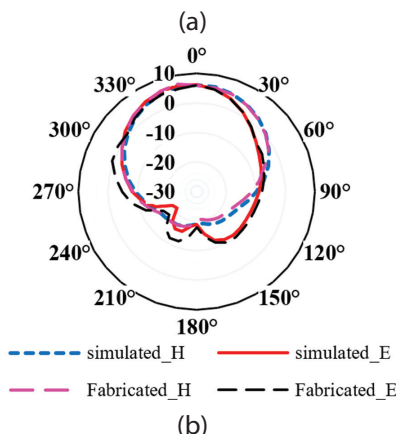


Fig. 15. Proposed fabricated antenna (a) setup of radiated power measuring with an anechoic chamber (b) radiation pattern of E- and H-plane (c) measured gain and radiation efficiency plot varies with frequency

Table 3. Comparisons between the suggested antenna and prior research

References	Overall size (mm*mm*mm)	Frequency (GHz)	S11 (dB)	Enhanced Gain (dB)	No. of EBG cells	Applications
[15]	7.5*6.1*0.13	28	-47.7	1.6	20	5G
[16]	40*40*2.2	6	-25	1.0	12	C band
[17]	101.4*313.8*2.2	3.25	-46.1	2.5	200	RCS reduction
[18]	70*70*1.6	5.2	--	2	28	WLAN
[19]	41.3*41.3*1.5	5.8	-12.5	1.9	40	ISM
[20]	58*58*3.81	5.8	-42	2.3	120	RFID
[28]	50*50*1.27	5.2	-28	1.1	72	WLAN
[29]	23*18*0.35	24	-23	2	24	IoT
[30]	68*73*3	5.2	-19.25	2.6	25	IoT
Proposed Work	40.8*50.5*1.6	5.2	-37.2	1.93	12	IoT

Table 3 shows the comparison of previous antenna designs incorporating EBG structures for IoT, 5G, and ISM applications. The previous studies indicate that using a larger number of EBG structures can enhance gain but often leads to increased design complexity. The proposed design uses fewer MEBG structures to achieve optimal gain. This suggested work balances the optimum performance and simple design that can be suitable for practical applications.

4. CONCLUSION

This paper discusses the limitations of traditional substrates, which are overcome by integrating the EBG structures to enhance the radiation performance of antennas. The proposed antenna is built on an FR-4 substrate with a thickness of 1.6 mm to mitigate the effect of surface wave propagation. Both MEBG and EEBG structures are examined to prevent the surface wave propagation around operating frequency 5.2 GHz. According to the examination, MEBG outperforms EEBG in suppressing surface wave propagation over a wider frequency range of 4.78–5.65 GHz with improved performance, whereas EEBG has a narrower bandgap of 4.97–5.41 GHz. The proposed antenna, which consists

of triple slots with only 12 MEBG unit cells, significantly improves the antenna parameters compared with conventional antenna while maintaining the compact size. The gain is improved substantially to 1.93 dB, and the return loss is greatly increased to 19.4 dB over the conventional antenna. The simulation results have been demonstrated and are consistent with fabrication results. The simple proposed design shows a high directivity of 7.51 dB, which can be suited for IoT-enabled applications such as home automation and industrial wireless monitoring.

Conflict of interest:

On behalf of all authors, the corresponding author states that there is no conflict of interest.

5. REFERENCES

- [1] L. Marco, P. Francesco, S. Domenico, "Internet of Things: A General Overview between Architectures Protocols and Applications", *Information*, Vol. 12, No. 2, 2021, p. 87.
- [2] D. Arnaoutoglou, T. Empliouk, T. Kaifas, M. Chrysomallis, G. Kyriacou, "A review of multifunctional antenna designs for the Internet of Things", *Electronics*, Vol. 13, No. 6, 2024, p. 3200.
- [3] Z. Wang, B. Yuan, X. Zhang, L. Guo, "An Axial-Ratio Beam-Width Enhancement of Patch-Slot Antenna Based on EBG", *Microwave and Optical Technology Letters*, Vol. 59, 2017, pp. 493-497.
- [4] M. Zambak, S. Al-Bawri, M. Jusoh, A. Rambe, V. K. Hamza, A. Almuhlaifi, M. Himdi, "A compact 2.4 GHz L-shaped microstrip patch antenna for ISM-band Internet of Things (IoT) applications", *Electronics*, Vol. 12, No. 9, 2023, p. 2149.
- [5] L. Anchidin, A. Lavric, M. Marian, A. Petrariu, V. Popa, "The design and development of a microstrip antenna for Internet of Things applications", *Sensors*, Vol. 23, No. 3, 2023, p. 1062.
- [6] Y. Madany, H. Elkamchouchi, H. A. Elmonieum, "High-Gain Pixel Patch Antenna Array for Miniature Wireless Communications and IoT Applications", *Progress In Electromagnetics Research C*, Vol. 131, 2023, p. 209-225.
- [7] A. Ayomikun, M. Mokayef, "Miniature microstrip antenna for IoT application", *Materials Today: Proceedings*, Vol. 29, 2020.
- [8] S. M. Refaat, A. Abdalaziz, E. K. I. Hamad, "Tri-Band Slot-Loaded Microstrip Antenna for Internet of Things Application", *Advanced Electromagnetics*, Vol. 10, No. 1, pp. 21-28.
- [9] Y. I. Ashyap et al. "An Overview of Electromagnetic Band-Gap Integrated Wearable Antennas", *IEEE Access*, Vol. 8, 2020, pp. 7641-7658.
- [10] D. Sievenpiper, L. Zhang, R. F. J. Broas, N. G. Alexopoulos, E. Yablonovitch, "High-impedance electromagnetic surfaces with a forbidden frequency band", *IEEE Transactions on Microwave Theory and Techniques*, Vol. 47, No. 11, 1999, pp. 2059-2074.
- [11] Y. Rahmat-Samii, F. Yang, "Microstrip Antennas Integrated with Electromagnetic Band-Gap (EBG) Structures: A Low Mutual Coupling Design for Array Applications", *IEEE Transactions on Antennas and Propagation*, Vol. 51, 2003 pp. 2936-2946.
- [12] Y. Li, K. Zhang, L. Yang, L. Du, "Gain enhancement and wideband RCS reduction of a microstrip antenna using triple-band planar electromagnetic band-gap structure", *Progress In Electromagnetics Research Letters*, Vol. 65, 2017, pp. 103-108.
- [13] P. P. Bhavarthe, S. S. Rathod, K. T. V. Reddy, "A Compact Dual Band Gap Electromagnetic Band Gap Structure", *IEEE Transactions on Antennas and Propagation*, Vol. 67, No. 1, 2019, pp. 596-600.
- [14] X. Tan, W. Wang, Y. Liu, A. Kishk, "Enhancing Isolation in Dual-Band Meander-Line Multiple Antenna by Employing Split EBG Structure", *IEEE Transactions on Antennas and Propagation*, Vol. 67, 2019, pp. 2769-2774.
- [15] A. Alsudani, H. Marhoon, "Design and Enhancement of Microstrip Patch Antenna Utilizing Mushroom Like-EBG for 5G Communications", *Journal of Communications*, Vol. 18, 2023, pp. 156-163.
- [16] M. Abdulhameed, M. M. Isa, M. Saari, Z. Zakaria, M. Mohsen, M. Attiah, "Mushroom-Like EBG to Improve Patch Antenna Performance for C-Band Satellite Application", *International Journal of Electrical and Computer Engineering*, Vol. 8, 2018, pp. 3875-3881.
- [17] Z. J. Han, W. Song, X. Q. Sheng, "Gain Enhancement and RCS Reduction for Patch Antenna by Using Polarization-Dependent EBG Surface", *IEEE Antennas and Wireless Propagation Letters*, Vol. 16, 2017, pp. 1631-1634.

- [18] P. Ketkuntod, T. Hongnara, W. Thaiwirot, P. Akkaraekthalin, "Gain enhancement of microstrip patch antenna using I-shaped Mushroom-like EBG structure for WLAN application", Proceedings of the International Symposium on Antennas and Propagation, Phuket, Thailand, 30 October - 2 November 2017, pp. 1-2.
- [19] S. Venkata, R. Kumari, "Gain and isolation enhancement of patch antenna using L-slotted mushroom electromagnetic bandgap", International Journal of RF and Microwave Computer-Aided Engineering, Vol. 30, 2020.
- [20] N. Melouki, A. Hocini, T. Denidni, "Performance enhancement of a compact patch antenna using an optimized EBG structure", Chinese Journal of Physics, Vol. 69, 2020.
- [21] N. Rao, D. Kumar, "Gain enhancement of microstrip patch antenna using Sierpinski fractal-shaped EBG," International Journal of Microwave and Wireless Technologies, Vol. 7, 2015, pp. 1-5.
- [22] G. Chaduvula, B. Kumari, "Implementation of EBG Structure to Reduce Surface Wave Excitations for IoT Range Applications", Proceedings of the 2nd International Conference on Artificial Intelligence, Computational Electronics and Communication System, Manipal, India, 16-17 February 2023, p. 012038.
- [23] P. Bhavarthe, S. S. Rathod, K. Reddy, "A Compact Two Via Slot-Type Electromagnetic Bandgap Structure", IEEE Microwave and Wireless Components Letters, Vol. 27, No. 5, 2017, pp. 446-448.
- [24] E. Wang, Q. Liu, "GPS patch antenna loaded with fractal EBG structure using an organic magnetic substrate", Progress In Electromagnetics Research Letters, Vol. 58, 2016, pp. 23-28.
- [25] K. Peter, Z. Raida, Z. Lukes, "Design and optimization of periodic structures for simultaneous EBG and AMC operation", Proceedings of the 15th Conference on Microwave Techniques COMITE, Brno, Czech Republic, 19-21 April 2010, pp. 195-198.
- [26] E. R. Iglesias, L. I. Sanchez, J. L. V. Roy, E. G, "Size Reduction of Mushroom-Type EBG Surfaces by Using Edge-Located Vias", IEEE Microwave and Wireless Components Letters, Vol. 17, 2007, pp. 670-672.
- [27] R. Remski, "Analysis of Photonic Bandgap Surfaces Using Ansoft HFSS", Microwave Journal, Vol. 43, 2000.
- [28] N. Jaglan, S. Dev Gupta, "Surface waves minimisation in microstrip patch antenna using EBG substrate", Proceedings of the International Conference on Signal Processing and Communication, Noida, India, 16-18 March 2015, pp. 116-121.
- [29] W. May, I. Sfar, L. Osman, J. M. Ribero, "A Textile EBG-Based Antenna for Future 5G-IoT Millimeter-Wave Applications", Electronics, Vol. 10, No. 2, 2021, p. 154.
- [30] A. Ahmad, F. Faisal, S. Ullah, D. Choi, "Design and SAR Analysis of a Dual Band Wearable Antenna for WLAN Applications", Applied Sciences, Vol. 12, No. 18, 2022, p. 9218.